Available online at www.sciencedirect.com

ScienceDirect

Advances in Space Research 71 (2023) 129–143

ADVANCES IN SPACE RESEARCH (a COSPAR publication)

www.elsevier.com/locate/asr

Study of aerosol anomaly associated with large earthquakes ($M > 6$)

Soujan Ghosh [a,*], Sudipta Sasmal [b], Manish Naja [c], Stelios Potirakis [d,e], Masashi Hayakawa [f]

[a] Indian Centre for Space Physics, 43 Chalantika, Garia St. Road, Kolkata 700084, West Bengal, India
[b] Institute of Astronomy Space and Earth Science, AJ-316, Sector - II, Salt Lake, Kolkata 700091, West Bengal, India
[c] Aryabhatta Research Institute of Observational Sciences, Manora Peak, Nainital 263001, Uttarakhand, India
[d] Department of Electrical and Electronics Engineering, University of West Attica, Ancient Olive Grove Campus, 12244 Egaleo, Greece
[e] Institute for Astronomy, Astrophysics, Space Applications and Remote Sensing, National Observatory of Athens, Metaxa and Vasileos Pavlou, 15236 Penteli, Greece
[f] Hayakawa Institute of Seismo Electromagnetics Co. Ltd., UEC Alliance Center, 521, 1-1-1 Kojma-cho, Chofu, Tokyo 182-0026, Japan

Received 15 June 2022; received in revised form 15 August 2022; accepted 18 August 2022
Available online 25 August 2022

Abstract

We present the variation of unusual atmospheric phenomena, aerosols, to understand the preseismic irregularities for two major earthquakes in Japan. We consider aerosol optical depth and Angstrom exponent data retrieved from the Moderate Resolution Imaging Spectroradiometer (MODIS) instrument onboard the *Terra* satellite to establish possible connections between earthquakes and the generation of aerosols. Variation of the aerosol parameters shows significant changes before the April 15, 2016, Kumamoto earthquake ($M = 7.0, h = 10$ km) and the November 21, 2016, Fukushima earthquake ($M = 6.9$ and $h = 9$ km), where M indicates the Richter magnitude and h indicates the focal depth. To identify the source of the aerosol particles, we use the Hybrid Single-Particle Lagrangian Integrated Trajectory model (HYSPLIT-4). This model uses both Lagrangian and Eulerian approaches to compute trajectories and establish a source-receptor relationship. We compute backward trajectories to check whether the aerosol generated near the epicenter is due to the preseismic processes or is transported from other areas. From our results, we conclude the fine-mode aerosols are generated in the vicinity of the epicenter, 3–7 days before the earthquakes.

Keywords: Lithospheric-atmospheric-ionospheric coupling; Aerosol optical depth; Angstrom exponent; HYSPLIT-4

1. Introduction

Atmospheric aerosols are particles suspended in the air in the form of a solid or liquid. They play an important role in climate change, atmospheric dynamics, weather change, and human health. These aerosols can be produced from two types of sources: (i) biogenic and (ii) anthropogenic. Natural aerosols are mainly sea salt and dust, whereas anthropogenic aerosols are mostly carbonaceous. A significant amount of tropospheric aerosol is anthropogenic and is created because of different processes, mainly industrialization. Aerosols act as cloud condensation nuclei and influence the climate by the direct and indirect methods of scattering of sunlight and changing cloud optical properties. They also regulate the energy balance of Earth, which has a great impact on climate variability (Zhao et al., 1988; Charlson et al., 1990; Jacobson, 2001; Jacobson, 2002; Lohmann and Lesins, 2002; Huebert et al., 2003; Andreae et al., 2005). As mentioned, aerosols can influence the climate by backscattering and absorption of radiation (direct method) and by changing the properties of clouds (indirect method). Positive and negative forcing result in net warming and net cooling on the surface of

* Corresponding author.
E-mail addresses: soujanghosh89@gmail.com (S. Ghosh), manish@aries.res.in (M. Naja), spoti@uniwa.gr (S. Potirakis), hayakawa@hi-seismo-em.jp (M. Hayakawa).

https://doi.org/10.1016/j.asr.2022.08.051
0273-1177/

Earth. Carbonaceous aerosols and mineral dust are responsible for warming, whereas sulfates and sea salts act as agents that cool the climate system (Charlson and Heintzenberg, 1995). The current economic upswing in the Asian region is the most significant cause of an increase in anthropogenic aerosols. Agricultural activities and biomass burning are also contributing significantly to the aerosol concentration in this region (Venkataraman et al., 2006; Kumar et al., 2011). Together they create mixed aerosol characteristics in the entire Asian region. The increase in atmospheric aerosols influences climatological variability as well as human health. Long-term observation of aerosols and their precursors has been conducted to understand the diurnal and annual variation and their chemical constituents along with the consequences for different climatological events and human health (Naja et al., 2014; Greenstone et al., 2015; Ghude et al., 2016; Joshi et al., 2016). Aerosol optical depth (AOD) is a measure of aerosols (urban haze, smoke particles, desert dust, and sea salt) distributed within a column of air from the instrument (Earth's surface) to the top of the atmosphere.

The physical and chemical processes associated with pre-earthquake processes are a complex, inhomogeneous, multidimensional, and multiparametric problem, as reported earlier (Pulinets and Boyarchuk, 2004; Molchanov and Hayakawa, 2008; Ouzounov et al., 2018). Thus, the precursory framework of seismic hazards involves many chemical, thermal, acoustic, and electromagnetic phenomena having a wide range of parameters. To achieve such thought and to validate this thought with significant variabilities of such parameters, a unified concept is proposed of coupling in various layers of the atmosphere and ionosphere due to seismic events through various channels (Pulinets and Boyarchuk, 2004; Molchanov, 2009; Pulinets and Ouzonov, 2011). This mechanism is known as lithospheric-atmospheric-iono spheric coupling (LAIC). As per the mechanism, several geochemical and geophysical processes are interrelated and connected with earthquake events. The initial geochemical and physical processes start with radon emanation (Omori et al., 2007). This radon is the primary source of air ionization in the near-surface area. Ions generated in this process coagulate with water molecules and start forming ion clusters. As the ion clusters of a few nanometers are injected into the atmosphere, the natural air conductivity profile changes, and this leads to a change of the ionospheric potential (Klimenko et al., 2011; Pulinets and Ouzonov, 2011). Hence, these continuous changes are reflected in the ionosphere as seismogenic ionospheric perturbations (Hayakawa et al., 1996a; Hayakawa et al., 1996b; Sasmal and Chakrabarti, 2009; Chakrabarti et al., 2010; Sasmal et al., 2014; Chakraborty et al., 2017; Ghosh et al., 2017; Asano and Hayakawa, 2018; Chakraborty et al., 2018; Hayakawa et al., 2018; Ghosh et al., 2019; Biswas et al., 2020). So from the mechanism explained above, we can expect a variation in the aerosol concentration associated with large seismic activities.

Initially, Tributsch (1978) found the interrelationship of aerosol anomalies and earthquakes. Pulinets et al. (1994) made the first attempt to describe seismo-ionospheric coupling using aerosols, natural radioactivity, and atmospheric electricity. The generation and the transportation were explained by application of the theory of a dirty plasma (Kikuchi, 1991). This emphasizes the consequences of two simultaneous processes: the generation of piezoelectric fields and the fluidity of hard materials. Microparticles are created because of the fluidity effect and accelerated movement is observed because of the electric reconnection effect of the piezoelectric fields. These aerosols change the conductivity profile of the atmosphere and are finally injected into the ionosphere, creating ionospheric perturbations. Atmospheric turbulence and the generation of thermospheric winds, increase in the atmospheric conductivity profile and the associated ion acceleration, and penetration of electric fields are mainly behind aerosol transportation to ionospheric heights. Later Araiza et al. (2006) used Aerosol Robotic Network (AERONET) information and found that the aerosol concentration increased during the San Simeon earthquake (California, USA). Okada et al. (2004) used SeaWiFS satellite data to study the aerosol anomaly for the Gujarat earthquake in 2001. They concluded that in the northeastern part of the Arabian Sea, AOD increased after the Gujarat earthquake and it was generated in the preparation zone of the earthquake as proposed by Dobrovolsky et al. (1979). Qin et al. (2014) used Moderate Resolution Imaging Spectroradiometer (MODIS) aerosol data from the *Terra* and *Aqua* satellites to find a possible effect of the 2008 Wenchuan earthquake. From their study, it was found that AOD locally increased 7 days before the 2008 Wenchuan earthquake near the active faults. They also reported that the increase of the AOD was related to the positive and negative ionospheric perturbations and was also associated with atmospheric anomalies. Pulinets et al. (2014) obtained AOD in 1020 nm data from AERONET for three earthquakes with magnitudes ranging from 5.8 to 7.1, and found abnormal behavior before those earthquakes. AOD during the 2015 Nepal earthquake was studied by Ganguly (2016) using *Terra* MODIS data, and increases in AOD of 0.9 and 0.6 were reported at 550 nm before and after the main shock, respectively. Phanikumar et al. (2018) presented the unusual variation of mesospheric ozone and its correlation with a very low frequency signal anomaly before the 2015 Nepal earthquake. A strong shift in the terminator time of the very low frequency signal amplitude was observed during the Nepal earthquake. This shift was strongly related to the mesospheric ozone anomaly. HYSPLIT-4 is a model developed by the National Oceanic and Atmospheric Administration (NOAA) to compute the trajectories of air parcel movements as well as the transportation, dispersion, and deposition of various chemical constituents (Draxler and Hess, 1998). Several studies have been conducted on anomalous aerosol increase and trajectories using the Hybrid Single-Particle Lagrangian

Integrated Trajectory (HYSPLIT) model (Li et al., 2015; Zhao et al., 2015). Okada et al. (2004) computed the backward trajectories for the 2001 Gujarat earthquake and found that the increase in aerosol parameters over the Arabian Sea was transported from the earthquake region.

In this article, we study the Kumamoto and Fukushima earthquakes of 2016. To investigate possible preseismic and co-seismic aerosol increase, we compute the aerosol anomaly from satellite data and present the conventional spatiotemporal variation of the anomaly by removing the background variation of the nonseismic condition. Our main aim is to find the anomaly variation of atmospheric aerosols before earthquakes to establish the hypothesis of the possible coupling mechanism during preseismic conditions. We have also checked that these aerosols are generated in the preparation zone or are transported from other places. Earlier work successfully observed a variety of parameters that are found to be very significant in the context of preseismic and co-seismic anomalous behaviors. This covers most of the major channel of the LAIC mechanism. As mentioned in Section 1, aerosol is also found to be a potent source of seismogenic impressions. We chose the earthquakes in such a way where evidence of such seismogenic impressions is already established by use of other parameters. This will also enable us to study and compare a multiparametric approach for LAIC mechanisms (Sasmal et al., 2021; Biswas et al., 2022; Chowdhury et al., 2022; Hayakawa et al., 2022). This article is organized as follows: in Section 2 we present our observations and the methods for extracting the anomaly, in Section 3 we present the results and discuss our results, and in Section 4 we provide concluding remarks.

2. Data and methods

We chose the Kumamoto and Fukushima earthquakes of 2016 to investigate possible preseismic and co-seismic irregularities of aerosol parameters. In Fig. 1, we present the epicenters of the two earthquakes. In April 2016, a series of earthquakes struck Kumamoto City, Japan. The mainshock, of magnitude $M = 7.0$, hit on April 16, 2016, at 01:25 JST (April 15, 2016, 16:25 UTC) at a depth of 10 km, and was preceded by a foreshock of magnitude $M = 6.2$ on April 14, 2016, at 21:26 JST (12:26 UTC). On November 22, 2016, at 05:59 JST (November 21, 2016, 20:59 UTC) another earthquake of magnitude $M = 6.9$ occurred in Fukushima prefecture at a depth of 9 km. We present the details of these two earthquakes in Table 1.

To study the aerosol anomaly, we use two different parameters: AOD and the Angstrom exponent. We used the MODIS $1^\circ \times 1^\circ$ dark target AOD at 550 nm and "land only" Angstrom exponent data from the *Terra* satellite to investigate the possible correlation between the aerosol anomaly and large earthquakes. MODIS records data in 36 different spectral bands from 0.4 μm to 14.4 μm in three different resolutions: 250 m, 500 m, and 1000 m. MODIS AOD and Angstrom exponent data are available as both daily and monthly averages. In this study, we use daily average data only. We found that because of gaps between swath paths, several data points are missing. We used AOD as it gives information on the amount of aerosol, whereas the higher value of the Angstrom exponent provides information on dominating smaller aerosol particles and vice versa. The Angstrom exponent is defined as follows:

$$Angstrom\ exponent = -(\ln \tau_{0.412}/\ln \tau_{0.47})/(\ln 0.412/\ln 0.47), \quad (1)$$

where τ is the AOD at a particular wavelength.

To analyze the satellite data and identify the anomaly, first we followed the method proposed by Cui et al. (2017) and Tramutoli et al. (2013) for thermal and gaseous fields. Cui et al. (2017) studied CH_4 and CO variation during the 2008 Wenchuan earthquake and the 2013 Lushan earthquake from *Aqua* AIRS data and observed an anomaly due to a large amount of gas emitted along the fault line before and after the Wenchuan earthquake and 3 months before the Lushan earthquake. We calculated the anomaly using the equation

$$Anomaly(x,y,t) = \frac{[G(x,y,t) - G_{bac}(x,y,t)]}{\sigma(x,y,t)}, \quad (2)$$

where G_{bac} is the background data prepared as the mean from multiple nonseismic years. For the Kumamoto earthquake, we used data from 2014, 2017, and 2018 to prepare the background data, whereas for the Fukushima earthquake, the background data were prepared with 2015, 2018, and 2019 data. For the Kumamoto earthquake and the Fukushima earthquake, we considered different years to prepare the background data. A strong earthquake occurred within the grid area we considered when studying the Kumamoto earthquake in 2015. Similarly, for the grid area of the Fukushima earthquake, 2014 and 2017 are seismically active years. To eliminate the effect of earthquakes in the background data, we chose nonseismic year data for both grid areas. The background data were prepared with use of the following equation:

$$G_{bac}(x,y,t) = \frac{1}{N}\sum_{i=1}^{N} G_i(x,y,t). \quad (3)$$

For both cases studied, N is 3 and $\sigma(x,y)$ is the standard deviation of the gridded data described by the equation

$$\sigma(x,y,t) = \sqrt{\frac{\sum_{i=1}^{N}[G(x,y) - G_{bac}(x,y)]^2}{N-1}}. \quad (4)$$

Finally, we used the HYSPLIT-4 model of the NOAA Air Resources Laboratory to find the aerosol movement with the air parcel. The HYSPLIT model is a hybrid approach between Lagrangian and Eulerian methods. As the air parcel moves, the calculation of advection and diffusion using the moving frame of reference is done by the Lagrangian

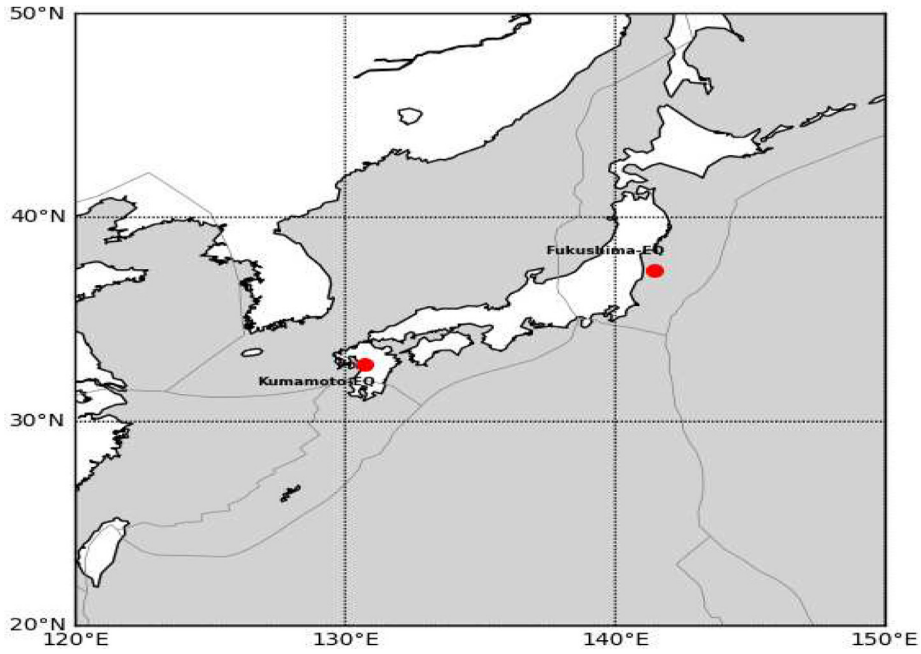

Fig. 1. The epicenters of the earthquakes marked with the red circles. Narrow gray lines are the tectonic plates boundaries. EQ: earthquake.

Table 1
Earthquake details.

Earthquake	Location of epicenter	Richter scale magnitude	Depth (km)	Date and time (UTC)	Radius of preparation zone (km)
Kumamoto earthquake	32.791° N 130.754° E	7	10	April 15, 2016, 16:25	1023.29
Fukushima earthquake	37.393° N 141.387° E	6.9	9	November 21, 2016, 20:59	926.82

method. The Eulerian method is used to compute air pollutant concentrations taking a fixed three-dimensional grid as a frame of reference (Stein et al., 2015). We aimed to investigate whether the anomalous aerosol variation in the vicinity of the earthquakes is due to transport of the aerosol from a distant place or is locally generated by seismogenic effects. The backward trajectory analysis provides insight and establishes a relationship between the aerosol particles at a particular location and the origin of those particles and their possible sources, commonly known as the source-receptor relation (Fleming et al., 2012). We used the backward trajectory for 24 h in the HYSPLIT-4 model along with the reanalysis data from the National Centers for Environmental Prediction and the National Center for Atmospheric Research (NCEP/NCAR) as input meteorological data to compute the air parcel movement. The NCEP/NCAR reanalysis data cover 2.5° global grids for different pressure levels. HYSPLIT uses the Lagrangian approach to calculate the dispersion by following the transport vector. For that computation, only meteorological parameters are used. HYSPLIT uses the same horizontal coordinate system and the projection of the meteorological input. According to the dispersion simulation, the particles are released from a particular source and follow the mean wind field. These particles are advected and dispersed because of the presence of atmospheric turbulence. The meteorological inputs are not readable in the HYSPLIT model, so a preprocessing program is required to convert the meteorological data fields into a standard format that is compatible with the HYSPLIT model. The computation of transportation and dispersion of particles using the HYSPLIT model generally uses one-hourly and three-hourly meteorological data. These data are then interpolated to achieve the required time by the HYSPLIT model. The system also includes a suite capability for running the model with real-time forecast meteorological data. This HYSPLIT model is also accessed through the Real-Time Environmental Applications and Display System (READY) (Rolph et al., 1993). The HYSPLIT output trajectories are drawn for the reference height 500 m above ground level from different heights. In general, the colors for 500 m, 1000 m and 1500 m are red, green, and blue. In our case we fixed the output level to 500 m so the HYSPLIT model presented the air parcel trajectories for each possible level to 500 m with different colors. The corresponding heights are automatically colored by the model itself.

3. Results and discussion

To present the result for both earthquakes, we use a spatiotemporal profile of the AOD anomaly and angstrom exponent as a function of the day number. For the Kumamoto earthquake, we used the spatial span of 125.5° E to 134.5° E and 28.5° N to 35.5° N for the period from April 1 to April 15, 2016. Fig. 2 presents the AOD anomaly for the Kumamoto earthquake. Along the *x*-axis and the *y*-axis, we present the longitude and the latitude, respectively, and the color bar represents the anomalies in AOD. The white lines are the country border, and the white dot marked with "K" is the earthquake epicenter. The first AOD anomaly is observed near the epicenter on April 3. The condition for such an anomaly in the next few days is unknown because of the lack of data. On April 10, we find an increase in the AOD, and it reaches its highest value on April 12. On April 14, the AOD anomaly is spread over the vicinity of the epicenter and further fades away.

For the Fukushima earthquake, we present a similar spatiotemporal profile of the AOD anomaly for the latitude-longitude region of 35.5° N to 40.5° N and 136.5° E to 145.5° E. The epicenter of the earthquake is marked with "F." In Fig. 3, we present the AOD anomaly variation from November 7 to November 21, 2016. From Fig. 3, it is observed that on November 13 the anomaly starts to increase and spread over the preparation zone of the earthquake. On November 21, 2016, a moderate anomaly is observed over the epicenter, and then it starts to decrease gradually.

In a similar way, in Figs. 4 and 5, we present the spatiotemporal variation of the Angstrom exponent over land as observed in the earthquake preparation zone for the Kumamoto earthquake and the Fukushima earthquake, respectively. Along the *x*-axis and the *y*-axis, we present the longitude and latitude, respectively, and the color bar represents the Angstrom exponent. Fig. 4 clearly shows that the Angstrom exponent is very high near the epicenter of the Kumamoto earthquake, which indicates a large number of small particles in that region at the time of the earthquake. On April 15, the angstrom exponent decreases, which indicates that large particles were injected into the atmosphere on that day. Fig. 5 shows that the Angstrom exponent is higher near the epicenter of the Fukushima earthquake, which indicates the dominance of smaller particles in the preparation zone for the Fukushima earthquake.

We also computed the percentage change in the AOD for both earthquakes around the epicenter. In Fig. 6, we present the percentage change in the AOD on anomalous days for the Kumamoto earthquake (left column) and the Fukushima earthquake (right column). The color bar represents the percentage increase in the AOD. On April 12 and 14, 2016, before the Kumamoto earthquake, an approximately 100%–150% change in the AOD is observed near the epicenter. For the Fukushima earthquake, and the greatest change in AOD is observed on November 13 and 14, 2016. On November 13, near the epicenter of the Fukushima earthquake, the greatest change is observed, around 170%, whereas for November 14, in the same region, the change is around 200%.

We present the backward trajectory results obtained for high AOD dates for both earthquakes. We constructed the matrix trajectory output for a 0.5° grid around the epicenter of the earthquakes from the HYSPLIT-4 model. In Figs. 7 and 8, we present the backward trajectories for both earthquakes. We tried to determine whether the unusual change in aerosols in the atmosphere is due to those seismic events or is due to transportation from other places and injection near the epicenter of the earthquakes or other reasons. We examined those 4 days of air parcel movement when the AOD anomaly is high. We draw back the trajectory starting from those grid points where the AOD anomaly is high. In Fig. 7, we present the HYSPLIT model output of air parcel movement during the Kumamoto earthquake for April 3, 10, 12, and 14, 2016. On April 3, the aerosol particles moved near the epicenter from the south and southeast, whereas on April 10 and 12, the movement is mainly from south of the epicenter. On April 14, the air parcel movement is from northwest of the epicenter. But the model output also reveals that the aerosols are generated within the vicinity of the epicenter. In Fig. 8, we present the HYSPLIT model output of air parcel movement during the Fukushima earthquake. The air parcel movement for the Fukushima earthquake is rather complex. We present the air parcel movement for November 13, 14, 17, and 21, 2016. On November 13, the AOD increases because of the air parcel movement from west of the epicenter. On November 14 and 17, the air parcel movement is from the southeast and the northwest, respectively. It is also evident that on November 17, the aerosol is transported from a distant place, but for that particular day, the aerosol is also generated within the preparation zone. So the increase in the AOD on November 17 is actually due to the mixed effect of locally generated and transported aerosol. On November 21, the air parcel movement is from east of the epicenter. The HYSPLIT model reveals that the aerosol is generated in the adjunct area of the epicenter and the increase in AOD is not a result of long-distance transport of the particles.

We analyzed the Kumamoto and Fukushima earthquakes for the abnormal AOD variation in the vicinity of the epicenter. We used MODIS AOD and Angstrom exponent daily data to study the variation during these two earthquakes. On the basis of our study, we anticipate that before both earthquakes aerosol is possibly generated within the vicinity of the epicenters. To confirm that these aerosol particles are generated by seismogenic causes, we first created the background profile for the same grid for the nonseismic period. By subtracting the AOD profile for the earthquake period from the background variation, we defined an anomaly in AOD. We observed a significant increase in AOD before both earthquakes. To eliminate the possibility that these aerosol particles were generated in

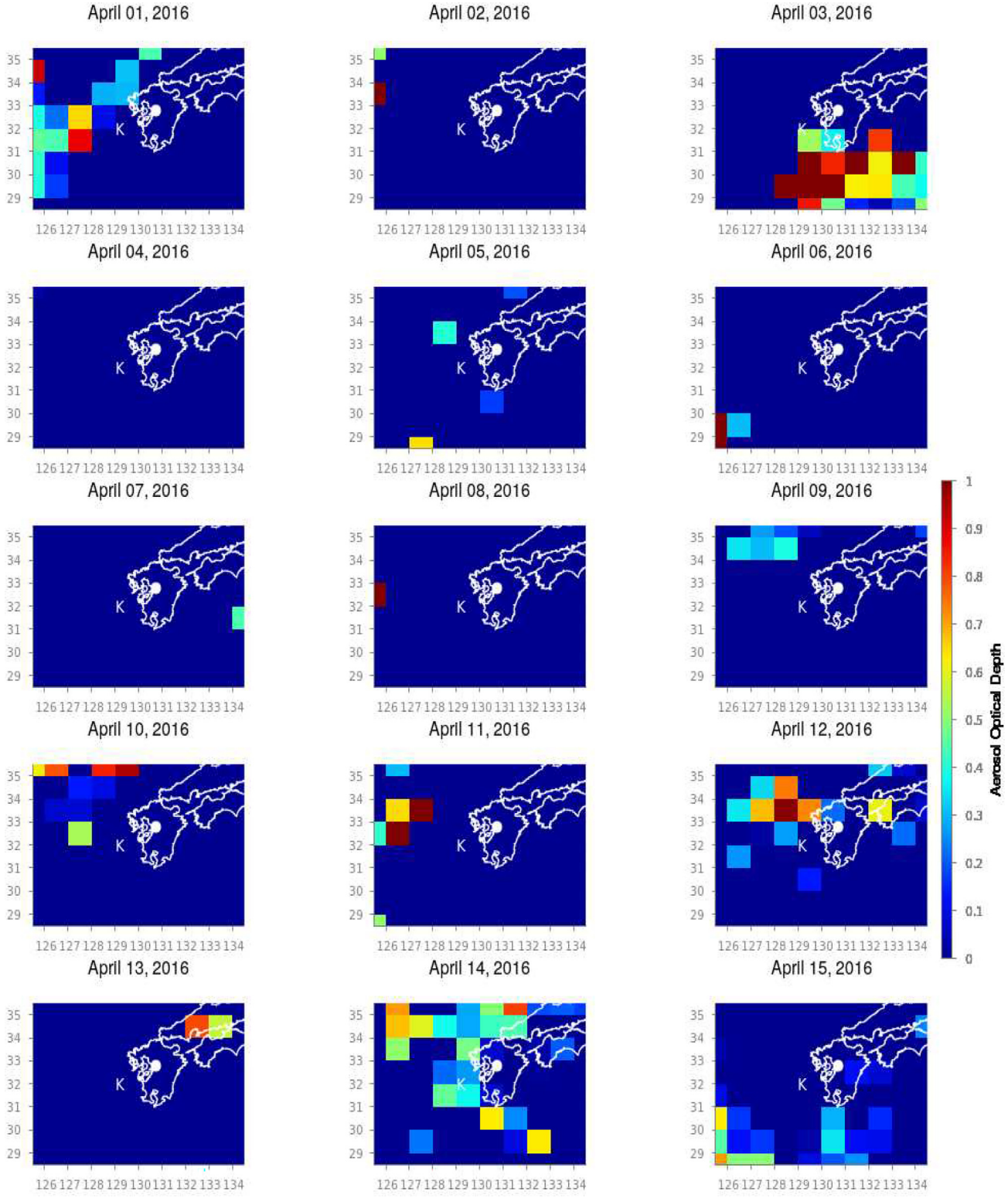

Fig. 2. Variation of aerosol optical depth anomaly from April 1 to April 15, 2016, for the Kumamoto earthquake.

other places for nonseismic reasons and then transported to the epicentral area, we used the HYSPLIT-4 model. We used this model to check the back trajectory of the air parcel movements. This trajectory reveals that the AOD anomaly just a few days before these earthquakes is locally generated. Our observation is found to be consistent with previous findings. Previously, several authors found aerosol anomalies before large earthquakes and established a relation between ionospheric and tropospheric anomalies. Qin et al. (2014) studied MODIS

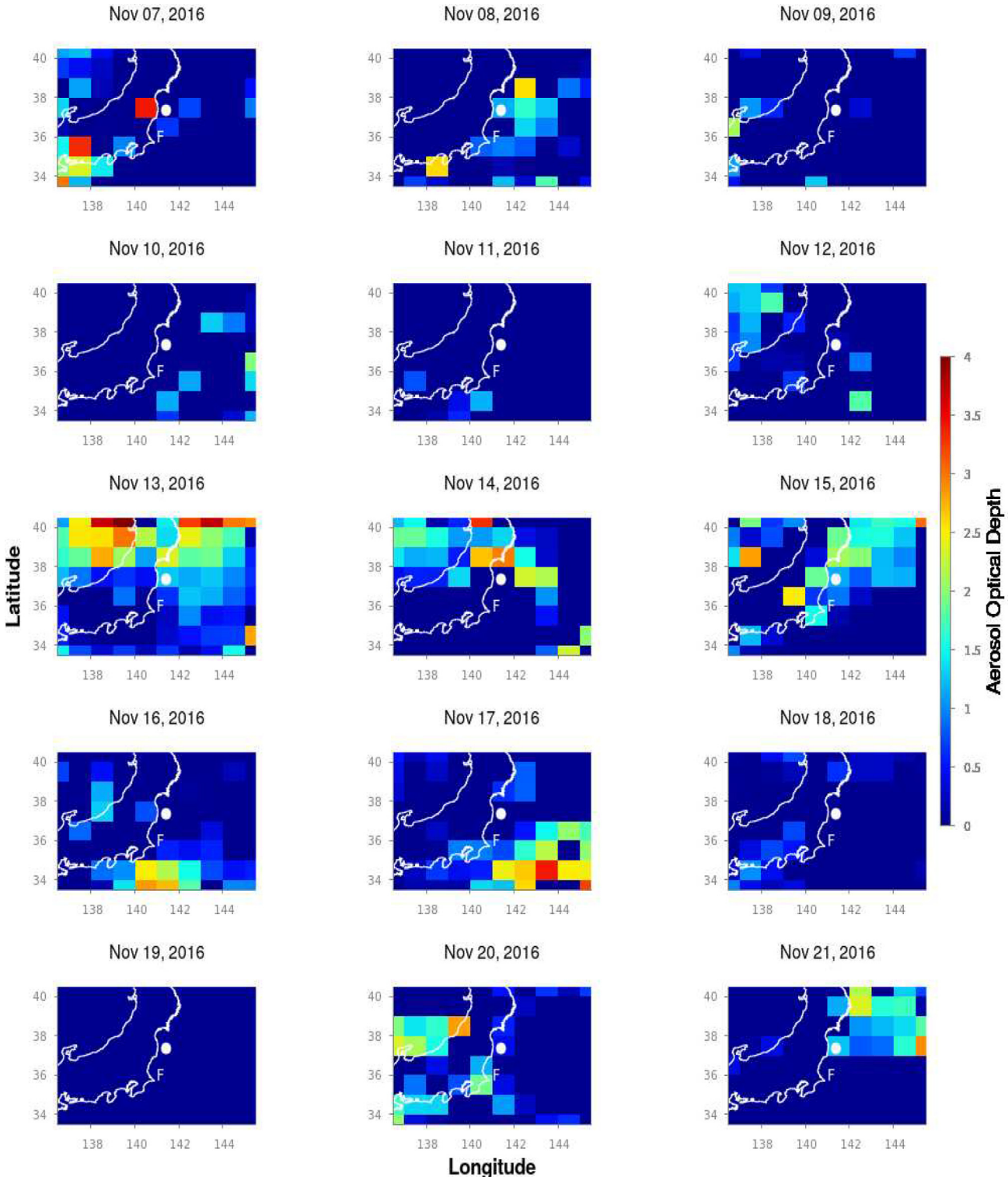

Fig. 3. Variation of aerosol optical depth anomaly from November 7 to November 21, 2016, for the Fukushima earthquake.

AOD data during the 2008 Wenchuan earthquake and found that the AOD was increased 7 days before the main-shock. It was reported that the AOD increased 1 day and 4 days before the negative and the positive ionospheric anomaly, respectively. They also found that the increase in AOD and other tropospheric parameters occurred exactly at the same time 1 day to 0 days before the earthquake. Liu et al. (2019) presented a comparative study of an aerosol anomaly during the 2008 Wenchuan earthquake and the 2013 Lushan earthquake. They observed anomalous behavior of the AOD 7 days and 4 days before the respective earthquakes. Similarly, we also tried to highlight

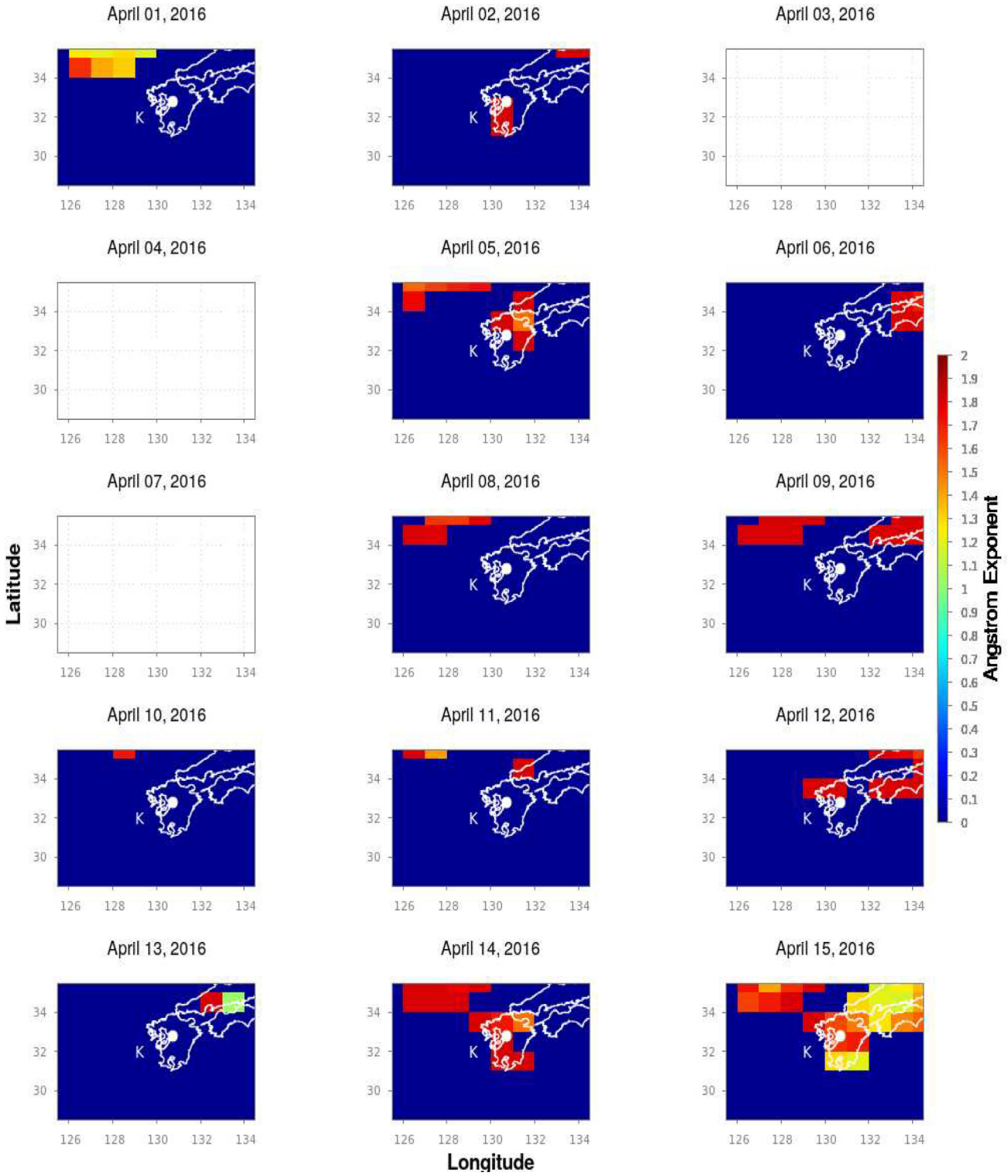

Fig. 4. Variation of the Angstrom exponent during the Kumamoto earthquake from April 1 to April 15, 2016.

several other anomalies that appear in different layers within the same period of the aerosol anomaly for these two earthquakes. This discussion of simultaneous anomalies appearing in other layers will establish the coupling mechanism described in the LAIC theory. In the case of the Kumamoto earthquake, Potirakis et al. (2018) used the very low frequency data from multiple stations and performed a critical analysis of ionospheric perturbations. They studied the nighttime fluctuation, trend, and dispersion, and found there was a clear preseismic anomaly before the earthquake. They also used a different method of criticality measurements to study the ionospheric anom-

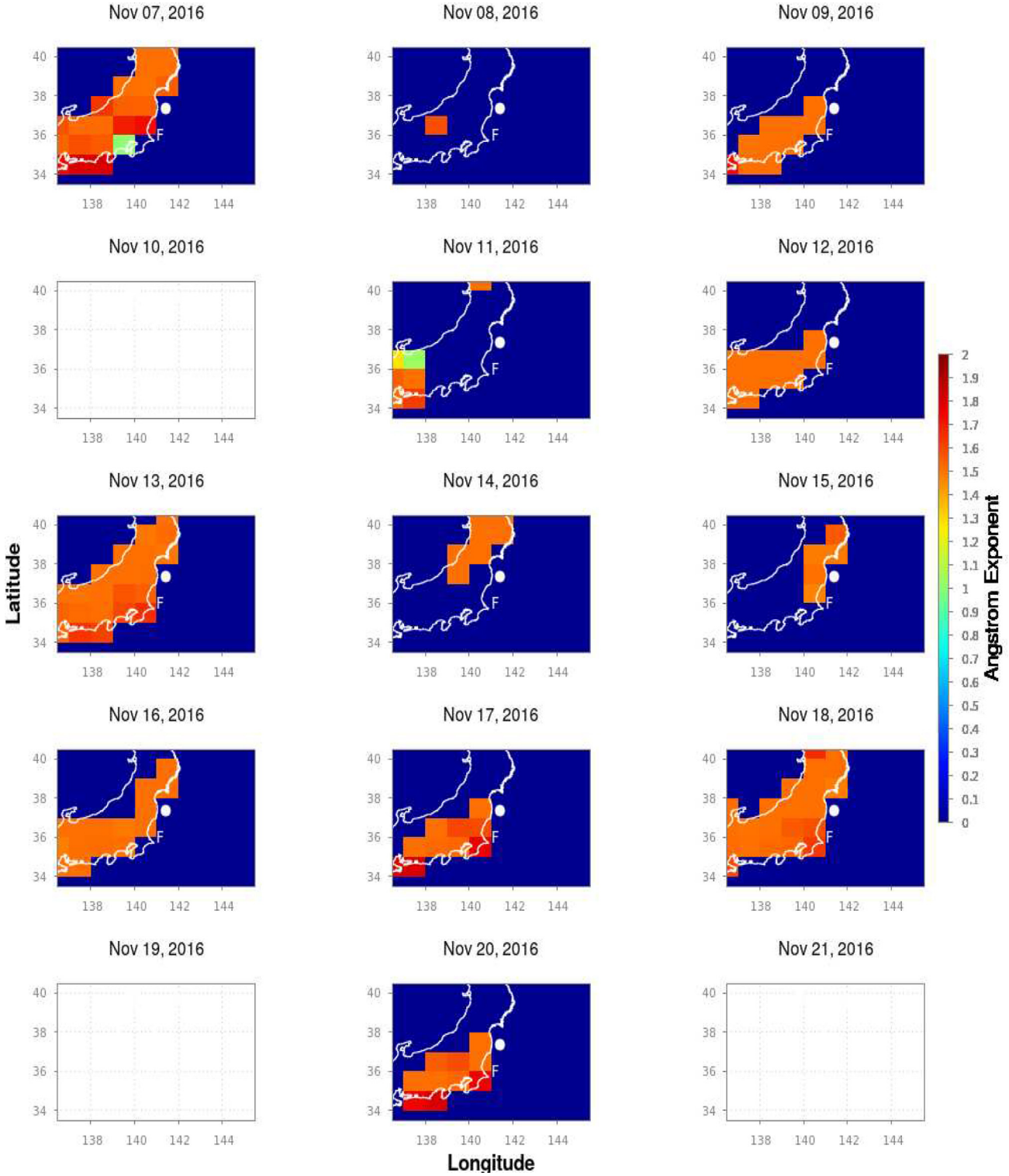

Fig. 5. Variation of the Angstrom exponent during the Fukushima earthquake from November 7 to November 21, 2016.

aly due to the Kumamoto earthquake, and found significant criticality 5–10 days for five very low frequency reception stations before the Kumamoto earthquake. Satellite data for various thermal parameters also showed irregularity before this earthquake. For the Kumamoto earthquake, the thermal parameter surface latent heat flux exhibited a maximum increase 5 days before (April 11, 2016) the mainshock, which was followed by a foreshock (April 14, 2016) (Ghosh et al., 2022). Yang et al. (2019) analyzed ERA5 data and revealed the presence of atmospheric gravity waves (AGWs) before the Kumamoto earthquake. The highest AGW activity was recorded on April 11, 2016,

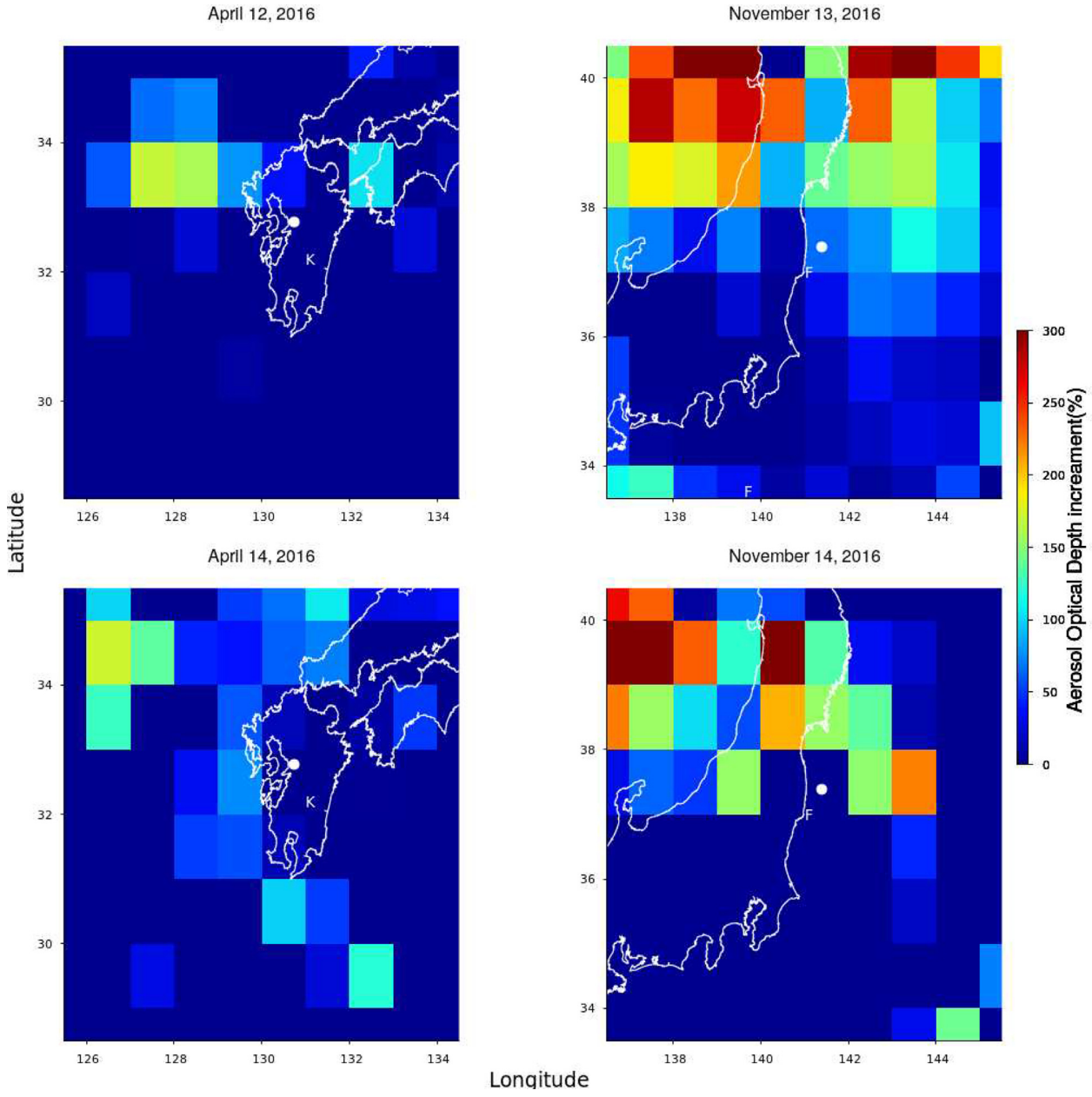

Fig. 6. Percentage change in aerosol optical depth on anomalous days for the Kumamoto earthquake (left) and the Fukushima earthquake (right).

i.e., 4 days before the mainshock. Kundu et al. (2022) also computed AGW activity from the SABER temperature profile, and found significant AGW activity 6 days to 4 days before the Kumamoto earthquake.

For the Kumamoto earthquake, the maximum AOD anomaly is observed on April 12 and 14, 2016. On April 12 and 14, the maximum AOD anomaly is obtained at 33.5° N and 128.5° E and at 30.5° N and 130.5° E with an amount of 0.9 and 0.62 with an increase of approximately 150% from the background values, respectively. The aerosol anomaly observed during the Kumamoto earthquake occurs during a period similar to that for other anomalies registered by various authors using various instruments. For the Fukushima earthquake, on November 13 and 14, anomalous AOD is observed near the epicenter. Output from the HYSPLIT model reveals that the increase in AOD is due to the aerosol generated in the preparation zone of the earthquake. This generation of aerosol particles can be associated with the seismic activity that occurred on November 21, 2016. On November 13 and 14, we observe an aerosol anomaly near the epicenter with AOD of 0.61 and 0.77, respectively. For the Fukushima earthquake, the aerosol anomaly is observed 1 week before the mainshock. A huge amount of aerosol is injected into the atmosphere on November 13, increasing the amount to around 150% of the background value. On November 14, the increase was around 200%, whereas on the day of the Fukushima earthquake an approximately 70% increase in

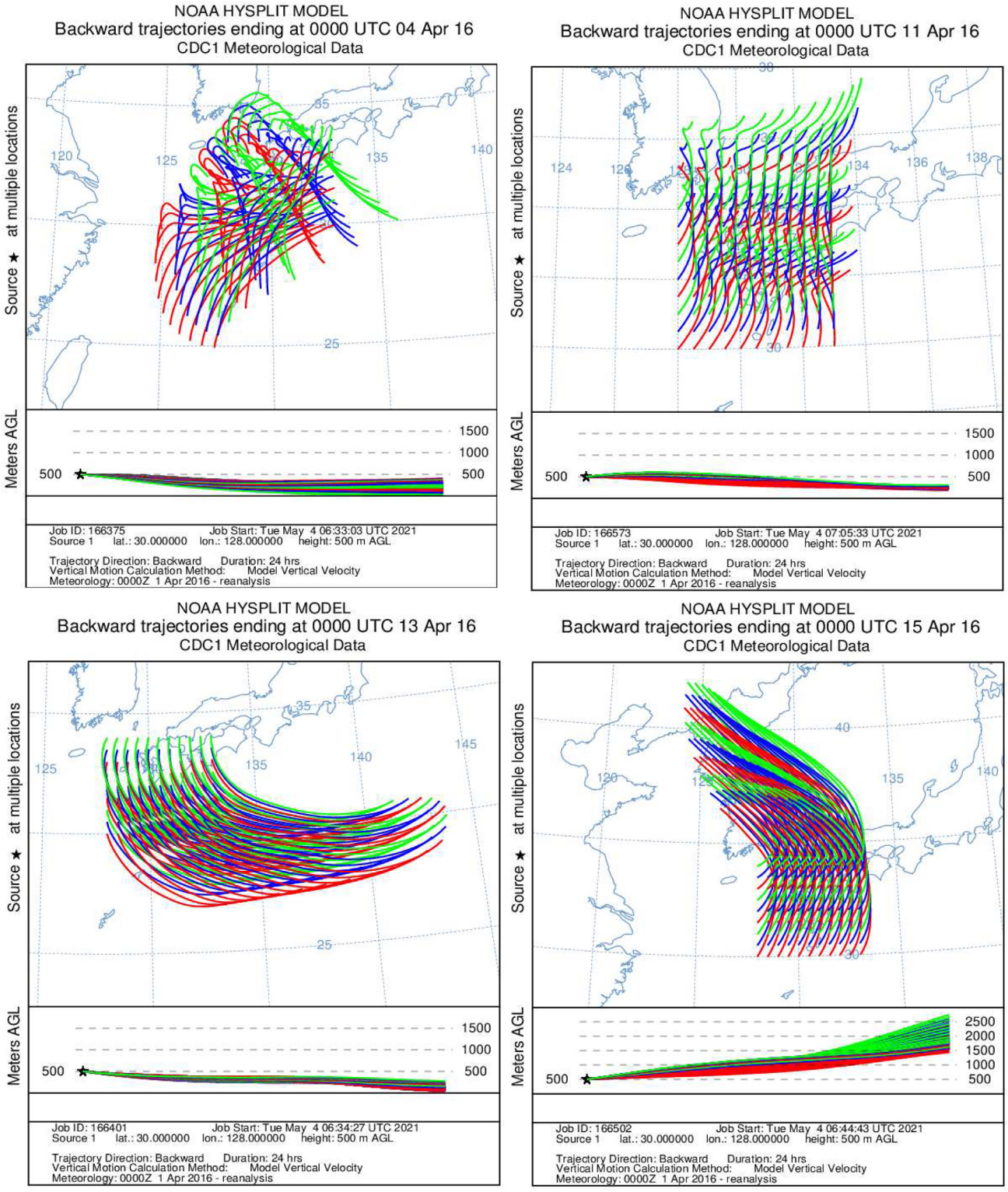

Fig. 7. HYSPLIT model output of air parcel backward trajectories for April 3, 10, 12, and 14, 2016, before the Kumamoto earthquake. AGL: above ground level; NOAA: National Oceanic and Atmospheric Administration.

the aerosol is observed. Angstrom exponent variation, on the other hand, reveals that during the Kumamoto and Fukushima earthquakes, the preparation zone is dominated by smaller particles. Although there are several successful observations of an aerosol anomaly during large earthquakes, some authors were unable to find a significant anomaly before the earthquake, and rather they reported an increase in AOD due to the dust generated in the fault

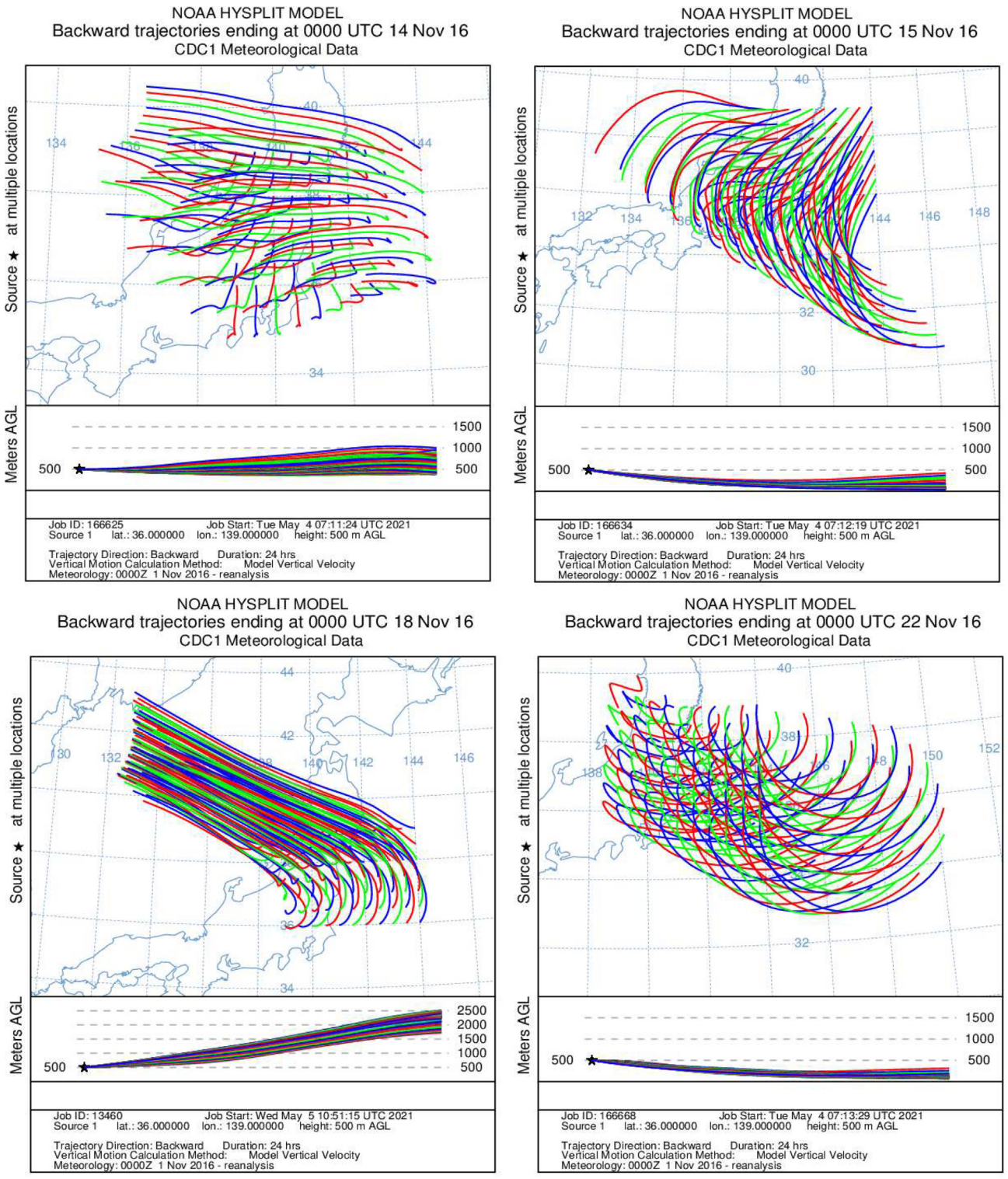

Fig. 8. HYSPLIT model output of air parcel backward trajectories for the Fukushima earthquake on November 13, 14, 17, and 21, 2016. AGL: above ground level; NOAA: National Oceanic and Atmospheric Administration.

regions after the mainshock. Okada et al. (2004) presented the change in aerosol parameters from SeaWiFS data and found that aerosol characteristics changed after the 2001 Gujarat earthquake. The HYSPLIT model output reveals that the increase in AOD in the northeastern part of the Arabian Sea is actually due to the transport of aerosol from the epicenter of the earthquake. Also, several atmospheric and meteorological parameters, as well as human activities, have large influences on aerosol parameters, which can change the effects significantly.

4. Conclusion

We analyzed the AOD and Angstrom exponent during two large earthquakes in Japan (Kumamoto and Fukushima). The aerosol parameters obtained from satellite observations show significant changes before these large earthquakes. It is well known that AOD also varies with the weather systems. But from our results, we observe an AOD anomaly related to the seismic events. Simultaneous satellite observation of thermal and chemical precursors for these two earthquakes also reveals a significant anomaly during the same timescale of the AOD anomaly. Ground-based observation of an ionospheric anomaly for these earthquakes establishes that the perturbation related to the earthquake percolates to ionospheric heights from the lower tropospheric region. These results indicate that geophysical and geochemical processes in the lithosphere during large earthquakes are closely related and the resulting signature can be found in the atmospheric and ionospheric regions that can be associated with the fundamental and revised thought of the LAIC mechanism. To understand the exact mechanism of geochemical and geophysical changes, we have to study the other channel of the LAIC mechanism—namely, the acoustic channel. Other satellite observations and simultaneous ground-based observations will help us to understand the role of the acoustic channel, mainly acoustic gravity waves, in the percolation of the particles to the upper layers. From this current study, we can conclude that the aerosol anomaly can also be used in short-term earthquake prediction as the anomalous behavior is observed 3–7 days before earthquakes. Regular study and monitoring of these parameters will help us to acquire knowledge for a more accurate precursory study for future earthquakes and their repercussions in atmospheric and ionospheric layers.

Declaration of Competing Interest

The authors declare that they have no known competing financial interests or personal relationships that could have appeared to influence the work reported in this paper.

Acknowledgments

SG and SS acknowledge the Government of West Bengal and DST-SERB (EMR/ 2016/003889) for financial support for the completion of the project. The authors also acknowledge MODIS and its scientific team for providing data.

References

Andreae, M.O., Jones, C.D., Cox, P.M., 2005. Strong present-day aerosol cooling implies a hot future. Nature 435, 1187–1190. https://doi.org/10.1038/nature03671.

Araiza Quijano, M.R., Leyva Contreras, A., Pelaez, J.N.C., Ivlev, L.S., Segovia, N., Pulinets, S., 2006. The aerosol of the vertical air column and its probable relationship to the seismic activity: Mexico City case of study. III Congreso Cubano de Meteorologia, 5–9, December, 2006, Capitolio de la Habana, La Habana, Cuba, CD Memories, ISBN 959-7160-31.

Asano, T., Hayakawa, M., 2018. On the tempo-spatial evolution of the lower ionospheric perturbation for the 2016 Kumamoto earthquakes from comparisons of VLF propagation data observed at multiple stations with wave-hop theoretical computations. Open J. Earthq. Res. 7 (3), 161–185. https://doi.org/10.4236/ojer.2018.73010.

Biswas, S., Kundu, S., Chowdhury, S., Ghosh, S., Yang, S., Hayakawa, M., Chakraborty, S., Chakrabarti, S., Sasmal, S., 2020. Contaminated effect of geomagnetic storm on pre-seismic atmospheric and ionospheric anomalies during imphal earthquake. Open J. Earthq. Res. 9. https://doi.org/10.4236/ojer.2020.95022.

Biswas, S., Chowdhury, S., Sasmal, S., Politis, D.Z., Potirakis, S.M., Hayakawa, M., 2020. Numerical modelling of sub-ionospheric very low frequency radio signal anomalies during the Samos (Greece) earthquake (M = 6.9) on October 30, 2020. Adv. Space Res. 70 (5), 1453–1471. https://doi.org/10.1016/j.asr.2022.06.016.

Chakrabarti, S.K., Sasmal, S., Chakrabarti, S., 2010. Ionospheric anomaly due to seismic activities-II: possible evidence from D-layer preparation and disappearance times. Nat. Hazards Earth Syst. Sci. 10, 1751–1757. https://doi.org/10.5194/nhess-10-1751-2010.

Chakraborty, S., Sasmal, S., Basak, T., Ghosh, S., Palit, S., Chakrabarti, S.K., Ray, S., 2017. Numerical modeling of possible lower ionospheric anomalies associated with Nepal earthquake in May, 2015. Adv. Space Res. 60 (8), 1787–1796. https://doi.org/10.1016/j.asr.2017.06.031.

Chakraborty, S., Sasmal, S., Chakrabarti, S.K., Bhattacharya, A., 2018. Observational signatures of unusual outgoing longwave radiation (OLR) and atmospheric gravity waves (AGW) as precursory effects of May 2015 Nepal earthquakes. J. Geodyn. 113, 43–51. https://doi.org/10.1016/j.jog.2017.11.009.

Charlson, R.J., Langner, J., Rodhe, H., 1990. Sulfate aerosol and climate. Nature 348, 22–24. https://doi.org/10.1038/348022a0.

Charlson, R.J., Heintzenberg, J. (Eds.), 1995. Aerosol Forcing of Climate. Wiley, New York.

Chowdhury, S., Kundu, S., Ghosh, S., Hayakawa, M., Schekotov, A., Potirakis, S.M., Chakrabarti, S.K., Sasmal, S., 2022. Direct and indirect evidence of pre-seismic electromagnetic emissions associated with two large earthquakes in Japan. Nat. Hazards 112, 2403–2432. https://doi.org/10.1007/s11069-022-05271-5.

Cui, Y., Ouzounov, D., Hatzopoulos, N., Sun, K., Zou, Z., Du, J., 2017. Satellite observation of CH_4 and CO anomalies associated with the Wenchuan M_S 8.0 and Lushan M_S 7.0 earthquakes in China. Chem Geol. 469, 185–191. https://doi.org/10.1016/j.chemgeo.2017.06.028.

Dobrovolsky, I.R., Zubkov, S.I., Myachkin, V.I., 1979. Estimation of the size of earthquake preparation zones. Pure Appl. Geophys. 117, 1025–1044. https://doi.org/10.1007/BF00876083.

Draxler, R.R., Hess, G.D., 1998. An overview of the HYSPLIT_4 modelling system for trajectories, dispersion, and deposition. Aust. Meteorol. Mag. 47, 295–308.

Fleming, Z.L., Monks, P.S., Manning, A.J., 2012. Review: untangling the influence of air-mass history in interpreting observed atmospheric composition. Atmos. Res. 104–105, 1–39. https://doi.org/10.1016/j.atmosres.2011.09.009.

Ganguly, N.D., 2016. Atmospheric changes observed during April 2015 Nepal earthquake. J. Atmos. Sol. Terr. Phys. 140, 16–22. https://doi.org/10.1016/j.jastp.2016.01.017.

Ghosh, S., Sasmal, S., Midya, S., Chakrabarti, S., 2017. Unusual change in critical frequency of F2 layer during and prior to earthquakes. Open J. Earthq. Res. 6, 191–203. https://doi.org/10.4236/ojer.2017.64012.

Ghosh, S., Chakraborty, S., Sasmal, S., Basak, T., Chakrabarti, S.K., Samanta, A., 2019. Comparative study of the possible lower ionospheric anomalies in very low frequency (VLF) signal during Honshu, 2011 and Nepal, 2015 earthquakes. Geomat. Nat. Hazards Risk 10 (1), 1596–1612. https://doi.org/10.1080/19475705.2019.1595178.

Ghosh, S., Chowdhury, S., Kundu, S., Sasmal, S., Politis, D.Z., Potirakis, S.M., Hayakawa, M., Chakraborty, S., Chakrabarti, S.K., 2022. Unusual surface latent heat flux yariations and their critical dynamics

revealed before strong earthquakes. Entropy 24 (1), 23. https://doi.org/10.3390/e24010023.
Greenstone, M., Nilekani, J., Pande, R., Ryan, N., Sudarshan, A., Sugathan, A., 2015. Lower pollution, longer lives. Econ. Political Wkly. 50 (8), 40–46.
Ghude, S.D., Chate, D.M., Jena, C., Beig, G., Kumar, R., Barth, M.C., Pfister, G.G., Fadnavis, S., Pithani, P., 2016. Premature mortality in India due to PM 2.5 and ozone exposure. Geophys. Res. Lett. 43, 4650–4658. https://doi.org/10.1002/2016GL068949.
Hayakawa, M., Molchanov, O.A., Ondoh, T., Kawai, E., 1996a. Anomalies in the sub-ionospheric VLF signals for the 1995 Hyogo-ken Nanbu earthquake. J. Phys. Earth 44, 413–418. https://doi.org/10.4294/jpe1952.44.413.
Hayakawa, M., Molchanov, O.A., Ondoh, T., Kawai, E., 1996b. The precursory signature effect of the Kobe earthquake on VLF subionospheric signals. J. Commun. Res. Lab. 43 (2), 169–180.
Hayakawa, M., Potirakis, S.M., Saito, Y., 2018. Possible relation of air ion density anomalies with earthquakes and the associated precursory ionospheric perturbations: An analysis in terms of criticality. Int. J. Electron. Appl. Res. 5 (2), 56–75. https://doi.org/10.33665/IJEAR.2018.v05i02.004.
Hayakawa, M., Schekotov, A., Izutsu, J., Yang, S.-S., Solovieva, M., Hobara, Y., 2021. Multi-parameter observations of seismogenic phenomena related to the Tokyo earthquake (M = 5.9) on 7 October 2021. Geosciences 12, 265. https://doi.org/10.3390/geosciences12070265.
Huebert, B.J., Bates, T., Russell, P.B., Shi, G., Kim, Y.J., Kawamura, K., Carmichael, G., Nakajima, T., 2003. An overview of ACE-Asia: strategies for quantifying the relationships between Asian aerosols and their climatic impacts. J. Geophys. Res. 108 (D23), 8633. https://doi.org/10.1029/2003JD003550.
Jacobson, M.Z., 2001. Strong radiative heating due to the mixing state of black carbon in atmospheric aerosols. Nature 409, 695–697. https://doi.org/10.1038/35055518.
Jacobson, M.Z., 2002. Control of fossil-fuel particulate black carbon and organic matter, possibly the most effective method of slowing global warming. J. Geophys. Res. 107 (D19), 4410. https://doi.org/10.1029/2001JD001376.
Joshi, H., Naja, M., Singh, K.P., Kumar, R., Bhardwaj, P., Suresh Babu, S., Satheesh, S.K., Krishna Moorthy, K., Chandola, H.C., 2016. Investigations of aerosol black carbon from a semi-urban site in the Indo-Gangetic Plain region. Atmos. Environ. 125, 346–359. https://doi.org/10.1016/j.atmosenv.2015.04.007.
Kikuchi, H., 1991. Meteorologico-electric phenomena and electrohydrodynamics (EHD) or electromagnetohydrodynamics (EMHD). In: Kikuchi, H. (Ed.), Environmental and Space Electromagnetics. Springer-Verlag, Tokyo.
Klimenko, M.V., Klimenko, V.V., Zakharenkova, I.E., Pulinets, S.A., Zhao, B., Tsidilina, M.N., 2011. Formation mechanism of great positive TEC disturbances prior to Wenchuan earthquake on May 12, 2008. Adv. Space Res. 48 (3), 488–499. https://doi.org/10.1016/j.asr.2011.03.040.
Kumar, R., Naja, M., Satheesh, S.K., Ojha, N., Joshi, H., Sarangi, T., Pant, P., Dumka, U.C., Hegde, P., Venkataramani, S., 2011. Influences of the springtime northern Indian biomass burning over the central Himalayas. J. Geophys. Res. 116 (D19), D19302. https://doi.org/10.1029/2010JD015509.
Kundu, S., Chowdhury, S., Ghosh, S., Sasmal, S., Politis, D.Z., Potirakis, S.M., Yang, S.S., Chakrabarti, S.K., Hayakawa, M., 2022. Seismogenic anomalies in atmospheric gravity waves as observed from SABER/TIMED satellite during large earthquakes. J. Sens. 2022, 3201104. https://doi.org/10.1155/2022/3201104.
Li, R., Gong, J., Zhou, J., Sun, W., Ibrahim, A.N., 2015. Multi-satellite observation of an intense dust event over southwestern China. Aerosol Air Qual. Res. 15, 263–270. https://doi.org/10.4209/aaqr.2014.02.0031.
Liu, Q., Shen, X., Zhang, J., Li, M., 2019. Exploring the abnormal fluctuations of atmospheric aerosols before the 2008 Wenchuan and 2013 Lushan earthquakes. Adv. Space Res. 63 (12), 3768–3776. https://doi.org/10.1016/j.asr.2019.01.032.
Lohmann, U., Lesins, G., 2002. Stronger constraints on the anthropogenic indirect aerosol effect. Science 298 (5595), 1012–1015. https://doi.org/10.1126/science.1075405.
Molchanov, O.A., Hayakawa, M., 2008. Seismo Electromagnetics and Related Phenomena: History and Latest Results, TERRAP, Tokyo.
Molchanov, O.A., 2009. Lithosphere-Atmosphere-Ionosphere Coupling due to Seismicity. In: Hayakawa, M. (Ed.), Electromagnetic Phenomena Associated with Earthquakes, Transworld Research Network, Trivandrum, pp. 255–279.
Naja, M., Mallik, C., Sarangi, T., Sheel, V., Lal, S., 2014. SO_2 measurements at a high altitude site in the central Himalayas: role of regional transport. Atmos, Environ. 99, 392–402. https://doi.org/10.1016/j.atmosenv.2014.08.031.
Okada, Y., Mukai, S., Singh, R.P., 2004. Changes in atmospheric aerosol parameters after Gujarat earthquake of January 26, 2001. Adv. Space Res. 33 (3), 254–258. https://doi.org/10.1016/S0273-1177(03)00474-5.
Omori, Y., Yasuoka, Y., Nagahama, H., Kawada, Y., Ishikawa, T., Tokonami, S., Shinogi, M., 2007. Anomalous radon emanation linked to preseismic electromagnetic phenomena. Nat. Hazards Earth Syst. Sci. 7, 629–635. https://doi.org/10.5194/nhess-7-629-2007.
Ouzounov, D., Pulinets, S., Hattori, K., Taylor, P. (Eds.), 2018. Pre-Earthquake Processes: A Multidisciplinary Approach to Earthquake Prediction Atudies, AGU Geophysical Monograph 234, Wiley.
Phanikumar, D.V., Maurya, A.K., Kumar, K.N., Venkatesham, K., Singh, R., Sharma, S., Naja, M., 2018. Anomalous variations of VLF subionospheric signal and mesospheric ozone prior to 2015 Gorkha Nepal earthquake. Sci. Rep. 8, 9381. https://doi.org/10.1038/s41598-018-27659-9.
Potirakis, S.M., Asano, T., Hayakawa, M., 2018. Criticality analysis of the lower ionosphere perturbations prior to the 2016 Kumamoto (Japan) earthquakes as based on VLF electromagnetic wave propagation data observed at multiple stations. Entropy 20 (3), 199. https://doi.org/10.3390/e20030199.
Pulinets, S.A., Legen'ka, A.D., Alekseev, V.A., 1994. Pre-earthquakes effects and their possible mechanisms. In: Kukuchi, H. (Ed.), Dusty and Dirty Plasmas, Noise and Chaos in Space and in the Laboratory. Plenum Publishing, New York, pp. 545–557.
Pulinets, S., Boyarchuk, K., 2004. Ionospheric Precursors of Earthquakes. Springer, Berlin. https://doi.org/10.1007/b137616.
Pulinets, S., Ouzonov, D., 2011. Lithosphere–atmosphere–ionosphere coupling (LAIC) model – an unified concept for earthquake precursors validation. J. Asian Earth Sci. 41 (4–5), 371–382. https://doi.org/10.1016/j.jseaes.2010.03.005.
Pulinets, S., Morozova, L., Yudin, I., 2014. Synchronization of atmospheric indicators at the last stage of earthquake preparation cycle. Res. Geophys. 4 (1). https://doi.org/10.4081/rg.2014.4898.
Qin, K., Wu, L.X., Ouyang, X.Y., Shen, X.H., Zheng, S., 2014. Surface latent heat flux anomalies quasi-synchronous with ionospheric disturbances before the 2007 Pu'er earthquake in China. Adv. Space Res. 53 (2), 266–271. https://doi.org/10.1016/j.asr.2013.11.004.
Rolph, G.D., McQueen, J., Draxler, R.R., 1993. Real-Time Environmental Applications and Display sYstem (READY). In: Proceedings of the Topical Meeting on Environmental Transport and Dosimetry, Charleston, S.C., American Nuclear Society, La Grange Park.
Sasmal, S., Chakrabarti, S.K., 2009. Ionosperic anomaly due to seismic activities – part 1: calibration of the VLF signal of VTX 18.2 KHz station from Kolkata and deviation during seismic events. Nat. Hazards Earth Syst. Sci. 9, 1403–1408. https://doi.org/10.5194/nhess-9-1403-2009.
Sasmal, S., Chakrabarti, S.K., Ray, S., 2014. Unusual behavior of very low frequency signal during the earthquake at Honshu/Japan on 11 March, 2011. Indian J. Phys. 88 (10), 1013–1019. https://doi.org/10.1007/s12648-014-0520-8.
Sasmal, S., Chowdhury, S., Kundu, S., Politis, D.Z., Potirakis, S.M., Balasis, G., Hayakawa, M., Chakrabarti, S.K., 2021. Pre-seismic irregularities during the 2020 Samos (Greece) earthquake (M = 6.9) as

investigated from multi-parameter approach by ground and space-based techniques. Atmosphere 12 (8), 1059. https://doi.org/10.3390/atmos12081059.

Stein, A.F., Draxler, R.R., Rolph, G.D., Stunder, B.J.B., Cohen, M.D., Ngan, F., 2015. NOAA's HYSPLIT atmospheric transport and dispersion modeling system. Bull. Am. Meteorol. Soc. 96 (12), 2059–2077. https://doi.org/10.1175/BAMS-D-14-00110.1.

Tramutoli, V., Aliano, C., Corrado, R., Filizzola, C., Genzano, N., Lisi, M., Martinelli, G., Pergola, N., 2013. On the possible origin of thermal infrared radiation (TIR) anomalies in earthquake-prone areas observed using robust satellite techniques (RST). Chem. Geol. 339, 157–168. https://doi.org/10.1016/j.chemgeo.2012.10.042.

Tributsch, H., 1978. Do aerosol anomalies precede earthquakes? Nature 276, 606–609. https://doi.org/10.1038/276606a0.

Venkataraman, C., Habib, G., Kadamba, D., Shrivastava, M., Leon, J.F., Crouzille, B., Boucher, O., Streets, D.G., 2006. Emissions from open biomass burning in India: integrating the inventory approach with high-resolution Moderate Resolution Imaging Spectroradiometer (MODIS) active-fire and land cover data. Glob. Biogeochem. Cycles 20 (2), 1–12. https://doi.org/10.1029/2005GB002547.

Yang, S.S., Asano, T., Hayakawa, M., 2019. Abnormal gravity wave activity in the stratosphere prior to the 2016 Kumamoto earthquake. J. Geophys. Res. Space Phys. 124 (2), 1410–1425. https://doi.org/10.1029/2018JA026002.

Zhao, D.W., Xiong, J.L., Xu, Y., 1988. Acid rain in southwestern China. Atmos. Environ. 22 (2), 349–358. https://doi.org/10.1016/0004-6981(88)90040-6.

Zhao, S., Yu, Y., Xia, D., Yin, D., He, J., Liu, N., Li, F., 2015. Urban particle size distributions during two contrasting dust events originating from Taklimakan and Gobi deserts. Environ. Pollut. 207, 107–122. https://doi.org/10.1016/j.envpol.2015.08.052.